Current Research in Materials Chemistry

Spectroscopic and Electrochemical Investigations of New 5-oxo-2-Phenyloxazol-4(5H)-ylidene Based Triazine Derivatives

Faheem Ahmad[1], Abdullah[1], M. Shaheer Akhtar[2], Hafiz Ghulam Abbas[3], Shabaz Alam[1], Hyung-Shik Shin[1,4*], Sadia Ameen[5*]

[1]*Energy Materials & Surface Science Laboratory, Solar Energy Research Center, School of Chemical Engineering, Jeonbuk National University, Jeonju, 54896, Republic of Korea.*

[2]*New & Renewable Energy Material Development Center (NewREC), Jeonbuk National University, Jeonbuk, Republic of Korea.*

[3]*Department of Nano science and Nanotechnology, Research Institute of Physics and Chemistry, Jeonbuk National University, Jeonju, 54896, Republic of Korea.*

[4*]*Korea Basic Science Institute (KBSI), 169-148 Gwahak-ro, Yuseong-gu, Daejon, 34133, Republic of Korea.*

[5*]*Advanced Materials and Devices Laboratory, Department of Bio-Convergence Science, Jeongeub Campus, Jeonbuk National University, 56212, Republic of Korea.*

Article Details

Article Type: Research Article
Received date: 02nd October, 2019
Accepted date: 26th October, 2019
Published date: 28th October, 2019

***Corresponding Author:** Sadia Ameen, Advanced Materials and Devices Laboratory, Jeongeub Industry-Academic Cooperation Support Centre, Jeongeub Campus, Jeonbuk National University, Republic of Korea. E-mail: sadiaameen@jbnu.ac.kr

*Hyung-Shik Shin, Energy Materials & Surface Science Laboratory, Solar Energy Research Center, School of Chemical Engineering, Jeonbuk National University, Jeonju, 54896, Yuseong-gu, Daejon, Republic of Korea. E-mail: hsshin@jbnu.ac.kr

Citation: Abdullah F, Abdullah, Akhtar MS, Abbas HG, Alam S, Shin HS, Ameen S (2019) Spectroscopic and Electrochemical Investigations of New 5-oxo-2-Phenyloxazol-4(5H)-ylidene Based Triazine Derivatives. Cur Res Mater Chem 1: 102. doi: https://doi.org/10.33790/crmc1100102.

Copyright: ©2019, This is an open-access article distributed under the terms of the Creative Commons Attribution License 4.0, which permits unrestricted use, distribution, and reproduction in any medium, provided the original author and source are credited.

Abstract

The present study reports the two step synthesis of a novel oxazolone derivative, 4-((4,6-bis(4-((Z)-(5-oxo-2-phenyloxazol-4(5H)-ylidene) methyl)phenoxy)-1,3,5-triazin-2-yl) oxy) benzaldehyde (CBOZ (5)), containing two oxazolone ring substituted with central triazine nucleus in their structural framework. The structural and spectroscopic properties of synthesized CBOZ (5) were characterized by FTIR, ^{1}HNMR, ^{13}CNMR, and mass spectroscopic analysis. The UV-Vis absorption of CBOZ (5) showed a single absorption band at ~370 nm due to π-π* transition with the estimated energy gap of ~3.02 eV. Cyclic voltammetry analysis revealed that the synthesized CBOZ (5) obtained the HOMO and LUMO values of -5.87 eV and-2.85 eV, respectively. Density functional theory (DFT) studies were carried out to predict the electronic absorption spectra of CBOZ (5) and the obtained values were in excellent agreement with the experimental results.

Keywords: Oxazolone, Electrochemical, Absorption properties, Photolumniscence, DFT study

Introduction

Nitrogen and oxygen heteroatoms based heterocyclic organic compounds are popularly known class of natural and the synthetic compounds, because of their unique optical and the electrical properties with enormous biological activities [1-6]. Oxazolone is a well-known five-membered heterocyclic compound containing nitrogen and oxygen atoms in their structural framework. Recently, oxazolone derivatives attained a considerable attention due to its versatile usage as an intermediate for the synthesis of varieties of organic motifs such as amino acids, amides, peptides, thiamines, N-substituted pyrroles, α-acylaminoalcohols, and other heterocyclic precursors [7-12]. Oxazolone derivatives have shown numerous biological properties such as anticancer, antimicrobial, antioxidant, anti-HIV, anti-inflammatory, anticonvulsant, antihypertensive, antagonistic and antiangiogenic, tyrosinase inhibitor, and cyclooxygenase-2 (COX-2) inhibitor properties which further enhance their importance in synthetic organic chemistry [13-20].

Oxazolone derivatives exhibit interesting photophysical and electrochemical properties and therefore, utilized as the promising materials for the electronic devices, biosensors, non-linear optical materials, and wide varieties of dyes [21-25]. The photophysical property is one of the important parameters of organic molecules for the potential applications in photonics and electronics [26, 27]. Several reports are available on the absorption and emission studies of differently substituted oxazolone derivatives like Murthy et al studied the photophysical behavior of five new oxazolone derivatives, which showed an intense absorption at 350-480 nm with the emission maxima at 390-535 nm [28]. In another work, Murthy and co-workers performed the photophysical studies of 4-(4′-N,N-dimethylbenzylidene)-2-phenyloxazol-5-(4H)-one and reported the absorption and emission maxima at ~465 and ~522 nm, respectively [23]. Ozturk et al reported the synthesis and the photophysical studies of four different oxazolone derivatives, substituted with N-phenyl-aza-15-crown-5 moiety which showed an intense visible absorption and an emission maxima in the range of 467-524 nm and 496-689 nm, respectively [29]. The versatile applicability of oxazolone molecule inspired us for assembling and decorating oxazolone molecule with diverse functional groups. In this work, a new oxazolone derivative, named as 4-((4,6-bis(4-((Z)-(5-oxo-2-phenyloxazol-4(5H)-ylidene) methyl)phenoxy)-1,3,5-triazin-2-yl) oxy)benzaldehyde (CBOZ (5), is synthesized containing the two oxazolone rings which are associated with a central triazine nucleus in their structural framework. To the best of our knowledge, for the first time, the synthesis of CBOZ (5) is reported and comprehensively characterized in terms of its structural, molecular, optical and electrochemical properties. To support our experimental studies, the theoretical calculations of optical and electrochemical properties are performed by DFT studies which are

in good agreement with the experimental results.

Experimental

Material and methods

All the reagents were purchased from TCI and Sigma-Aldrich as 'synthesis grade' and used without the further purifications. The progress of the reaction was monitored with the thin layer chromatography (TLC) plates of aluminum silica gel 60 F254 (Merck).

Synthesis of 4,4',4''-[1,3,5-triazine-2,4,6-triyltris(oxy)] tris-benzaldehyde (3)

The mixture of trichlorotriazine (1, 2 mmol), 4-hydroxybenzaldehyde (2, 6.17 mmol) and sodium carbonate in p-dioxane solvent was taken in a flask. The reaction mixture was stirred and refluxed under nitrogen atmosphere for 12 h. After completion of the reaction (as monitored by TLC), the reaction mixture was allowed to cool at the room temperature and poured into cold deionized (DI) water. The resulting precipitate was filtered off and washed with cold DI water to obtain the crude product. The crude product was subjected to column chromatography on silica gel with dichloromethane and hexane (1:1) to achieve the pure product (3). FTIR (KBr, cm^{-1}): 3018, 1722, 1644, 1595, 1406, 1292, 1216, 1167, 1056, 844, 778; ^{1}H NMR (400 MHz, $CDCl_3$, δ, ppm): 9.90 (s, 3H), 7.96 (d, 6H), 7.28 (d, 6H); ^{13}C NMR (100 MHz, $CDCl_3$, δ, ppm): 190.5, 173.2, 155.8, 134.4, 131.3, 122.6. MS (ESI) m/z: 441.10 $[M]^{+\bullet}$.

Synthesis of 4-((4,6-bis(4-((Z)-(5-oxo-2-phenyloxazol-4(5H)-ylidene)methyl)phenoxy) -1,3,5-triazin-2-yl)oxy)benzaldehyde, CBOZ (5)

In a dry flask, the mixture of aldehyde (3, 1 mmol), hippuric acid (4, 2.5 mmol) and sodium acetate (2.7 mmol) in acetic anhydride (20.0 mL) was heated under reflux for 2 h. After completion of the reaction, the reaction mixture was cooled, diluted with ethanol and kept overnight at the room temperature. The obtained solid was filtered, dried and purified by column chromatography to obtain the pure compound (5). FTIR (KBr, cm^{-1}): 3048, 2924, 1780, 1751, 1654, 1602, 1554, 1501, 1365, 1321, 1288, 1206, 1165, 847, 690; ^{1}H NMR (400 MHz, $CDCl_3$, δ, ppm): 9.91 (s, 1H), 8.22 (dd, 4H), 8.16 (dd, 2H), 8.02 (s, 2H), 7.88 (dd, 4H), 7.45-7.60 (m, 6H), 7.24 (dd, 2H), 7.16 (dd, 4H); ^{13}C NMR (100 MHz, $CDCl_3$, δ, ppm): 191.3, 175.9, 169.8, 167.9, 164.2, 158.4, 152.7, 133.8, 133.7, 133.0, 131.5, 131.0, 130.6, 129.2, 128.5, 126.1, 122.1, 122.0, 112.8. MS (ESI) m/z for $[C_{42}H_{25}N_5O_8]$: calculated 727.17; found 727.65 $[M]^{+\bullet}$.

Computational details

The geometry optimizations were performed using the Vienna ab-initio simulation package (VASP) [30,31]. The electron-ion interactions were described using the projector-augmented wave (PAW) method, which was primarily a frozen-core all-electron calculation [31]. The attractive Vander Waals interactions were included using Grimme's correction for PBE-D3 method [32]. For the structure optimization, atoms were relaxed in the direction of the Hellmann-Feynman force using the conjugate gradient method with an energy cut-off of ~400 eV until a stringent convergence criterion (of 0.02 eV/Å) was satisfied. The lattice constants were optimized using PBE-D3 exchange-correlation functional. The accurate electronic structure and optical calculations were performed using HSE06 functional [33]. By neglecting the local field effects, the imaginary part of the frequency-dependent dielectric matrix was determined from the equation:

$$\varepsilon_{\alpha\beta}^{2}(\omega)=\frac{4\pi^2e^2}{\Omega}\lim_{q\to 0}\frac{1}{q^2}\sum_{c,v,\mathbf{k}}2w_k\delta(\varepsilon_{c\mathbf{k}}-\varepsilon_{v\mathbf{k}}-\omega)<u_{c\mathbf{k}+\mathbf{e}_\alpha q}|u_{v\mathbf{k}}\rangle\langle u_{c\mathbf{k}+\mathbf{e}_\beta q}|u_{v\mathbf{k}}>^{*}$$

where, indices c and v refer to the conduction and valence band states, respectively; is the weight of the k-point; and uck is the cell periodic part of the orbitals at the k-point. The real part of the tensor was obtained from the Kramers-Kronig relation. The absorption and refractive index was calculated from the relation:

$$\alpha(\omega)=\frac{2\omega}{c}\sqrt{\frac{|\varepsilon(\omega)|+\varepsilon_1(\omega)}{2}},\quad \text{where,}\quad |\varepsilon(\omega)|=\sqrt{\varepsilon_1^{\,2}+\varepsilon_2^{\,2}}$$

$$n(\omega)=\frac{1}{\sqrt{2}}\sqrt{\frac{|\varepsilon(\omega)|+\varepsilon_1(\omega)}{2}}$$

Characterizations

Fourier transform infrared (FTIR) spectra were recorded in the 400-4000 cm^{-1} wave-number range by using FTIR-4100 (JASCO) spectrometer. ^{1}H NMR (400 MHz) and ^{13}C NMR (100 MHz) spectra were recorded through JEOL FT-NMR Spectrophotometer by using $CDCl_3$ as solvent. The chemical shifts (δ) were reported in ppm relative to TMS as an internal standard. The UV-Vis absorption and the photoluminescence spectrum were performed in chlorobenzene by using V-670 (JASCO) spectrophotometer and FP-6500 (JASCO) fluorometer, respectively. Cyclic voltammetry (CV) measurements were carried out by using an electrode system of WPG 100 Potentiostat/Galvanostat (WonA Tech). CV measurements were performed at a scan rate of 100 mV/s by using three-electrode cell system, containing a glassy carbon working electrode, a saturated calomel reference electrode (SCE) and a platinum wire counter electrode. Thermogravimetric analysis (TGA) was carried out under an inert atmosphere at a scan rate of ~10oC min-1 by using TA Q-50 Thermogravimetric Analyzer instrument. Differential scanning calorimetry (DSC) measurements were performed by DSC-2910 instrument at a heating and cooling rate of ~10 ^oC min^{-1} under nitrogen atmosphere.

Results and Discussion

Spectroscopic Studies

The synthesis of the target compound (5) was performed by the two step synthetic procedure, as depicted in Scheme 1. The intermediate (3) was synthesized by following the procedure as reported by Mikroyannidis et al [34]. The compound 5 was typically synthesized by cyclodehydration condensation reaction process which involved the intermediate (3) with hippuric acid in the presence of sodium acetate and acetic anhydride [20]. The structural descriptions of the synthesized CBOZ (5) are described on the basis of FTIR, ^{1}H NMR, ^{13}C NMR and Mass spectral studies which are found in good corroboration with the expected structural framework of the synthesized compound. The FTIR spectrum (ESI^+) displays the characteristic signals for $(C=O)_{ald}$, lactone carbonyl, -(C=N), (C-O) and (C-N) at ~1780, ~1751, ~1654, ~1206 and ~1165 cm^{-1}, respectively [35]. However, the absorption band resonating at around ~1602 cm^{-1} is assigned to the exocyclic double bond attached to the oxazolone ring [35]. ^{1}H NMR spectral analysis, as shown in Figure. 1(a), exhibits the singlet appearing at δ ~9.91 and ~8.02 which are attributed to the aldehydic and olefinic protons, respectively. The phenyl ring attached to the oxazolone ring shows the doublet (δ ~8.22) and multiplet peak (δ ~7.48-7.60), representing the two ortho protons and three (2 para and 1 meta) protons, respectively. However, the double doublets at δ ~8.16, ~7.88, ~7.24 and ~7.16 are assigned to the aromatic protons of benzene rings, substituted to triazine nucleus. From ^{13}C NMR spectral study (Figure. 1(b), the absorption band resonating at δ ~191.3 corresponds to carbonyl carbon of the aldehydic group, while the carbons of triaizne nucleus shows two different peaks at δ ~175.9 and ~169.4 due to the presence of two different substituents on the carbon atom of triazine. Similarly, the signals at δ ~167.9, ~164.0 and ~133.7 correspond to the carbonyl, C-10′ and C-12′ carbons of oxazolone ring, respectively [35]. The complete spectral assignment of CBOZ (5) is presented in Table S-1 and S-2, ESI^+.

CBOZ (5) shows m/z value at ~727.65, as depicted in Figure. S-2, ESI†, is found in good conformity with the proposed structure. All the above spectral assignment regarding the structure elucidation confirms the successful synthesis of CBOZ (5). The optimized molecular structure of CBOZ (5) is performed by DFT calculations in XY plane, as shown in Figure. 2, which would be discussed later under DFT study.

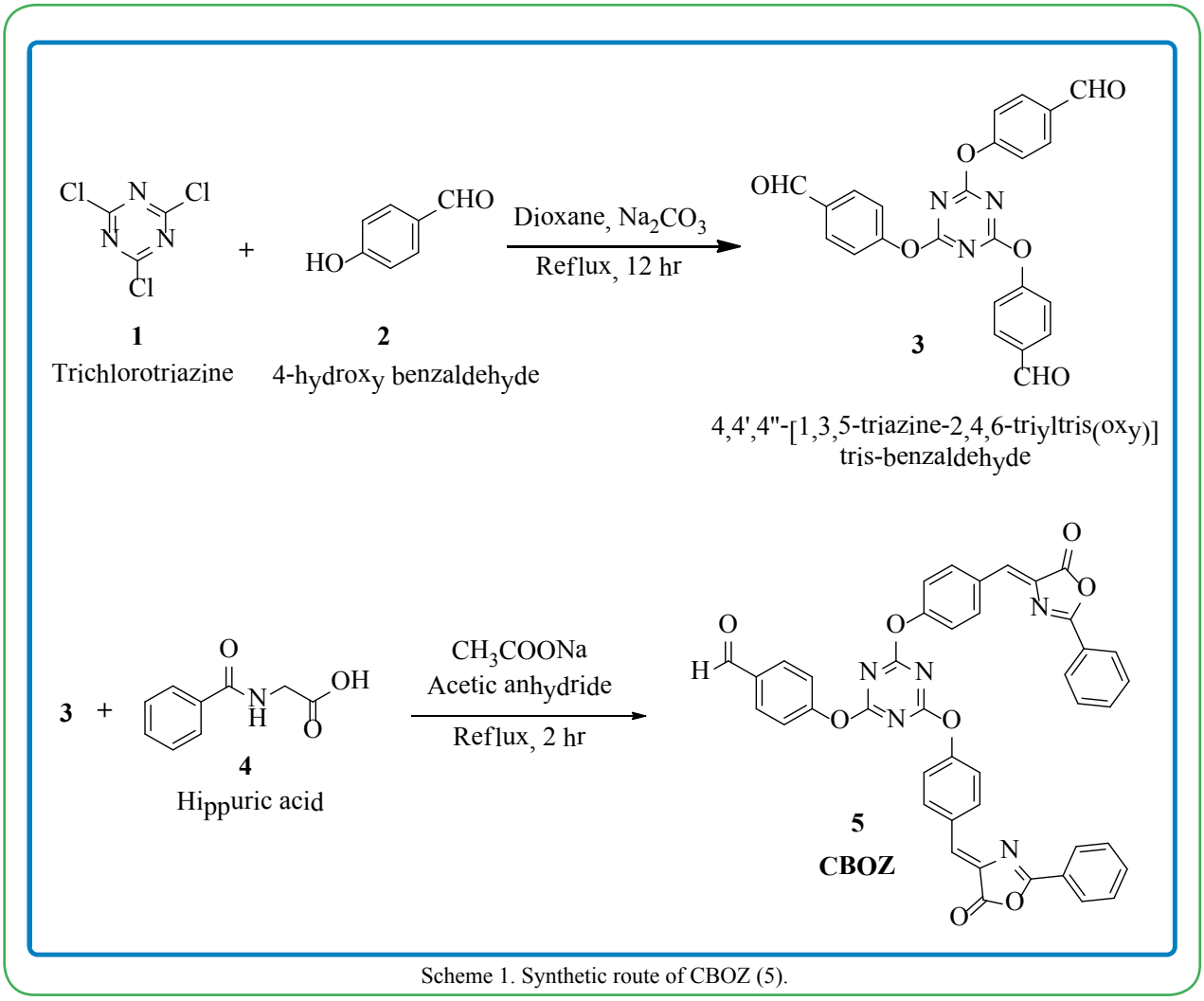

Scheme 1. Synthetic route of CBOZ (5).

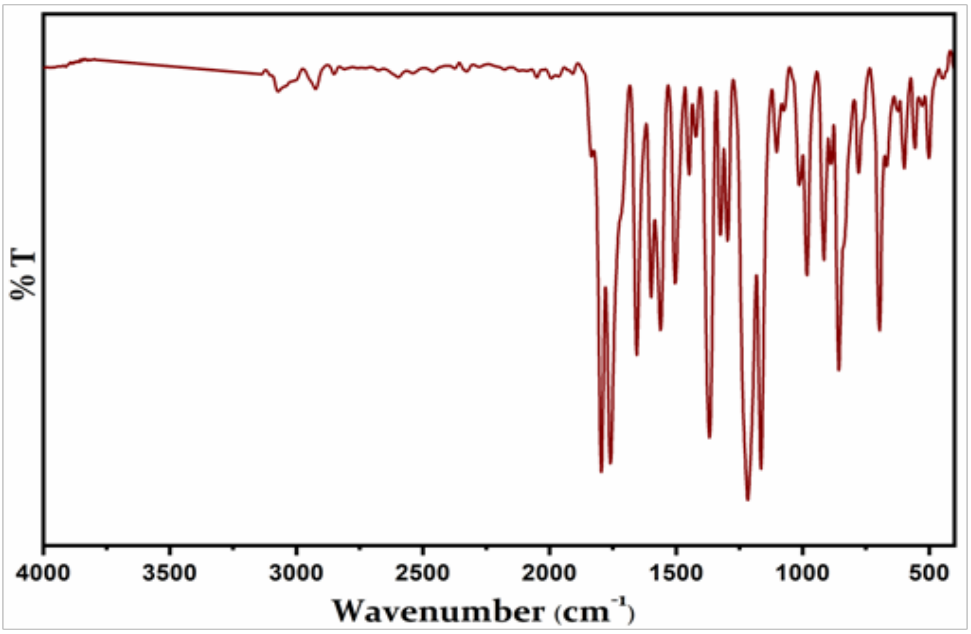

Figure S-1: FTIR spectrum of CBOZ (5)

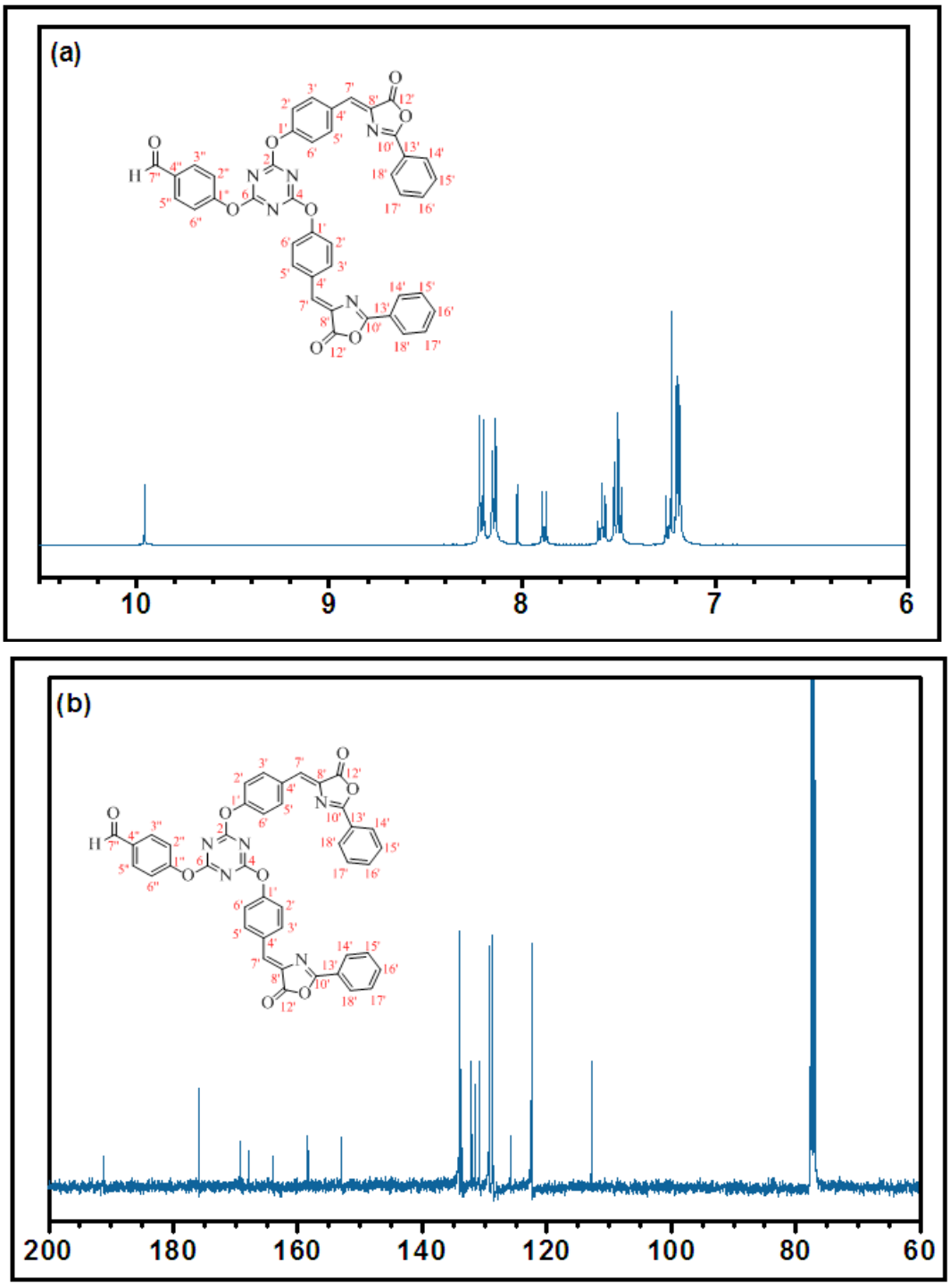

Figure. 1(a) ^{1}H NMR and (b) ^{13}C NMR spectrum of CBOZ (5).

Atom	Signals	Atom	Signals
H-7″	9.91, s, 1H	H-3′/H-5′	7.88, dd, 2H
H-3″/H-5″	8.15, dd, 2H	H-7′	8.02, s, 1H
H-2″/H-6″	7.24, dd, 2H	H-14′/H-18′	8.22, dd, 4H
H-2′/H-6′	7.19, dd, 2H	H-15′/H-16′/H-17′	7.48-7.60, m, 6H

Table S-1: ^{1}H NMR chemical shifts (δ/ppm) of CBOZ (5)

Atom	Signals	Atom	Signals
C2/C4	175.9	C4′	132.0
C6	169.4	C7′	112.8
C1″	158.4	C8′	133.7
C2″/C6″	122.6	C12′	167.9
C3″/C5″	133.5	C10′	164.0
C4′	134.0	C13′	125.8
C7″	191.3	C14′/C18′	128.7
C1′	152.9	C15′/C17′	129.2
C2′/C6′	122.4	C16′	131.5
C3′/C5′	130.8		

Table S-2: ^{13}C NMR chemical shifts (δ/ppm) of CBOZ (5)

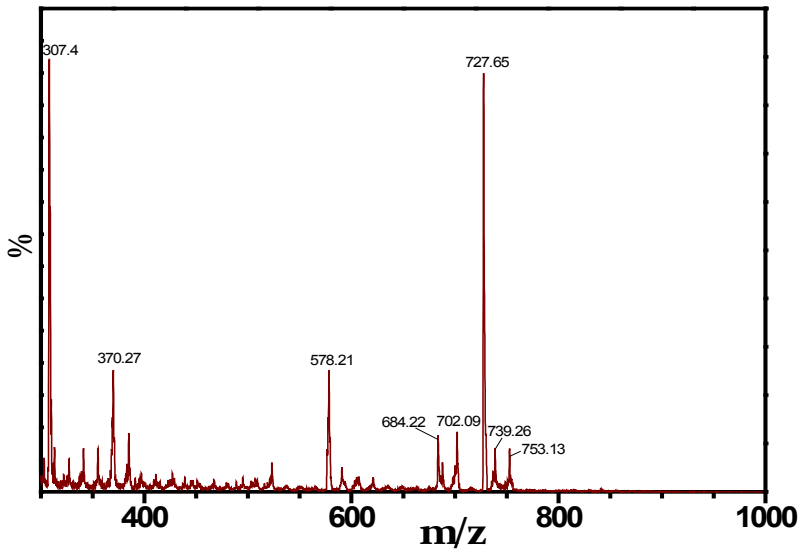

Figure. S-2: Mass spectrum of CBOZ (5)

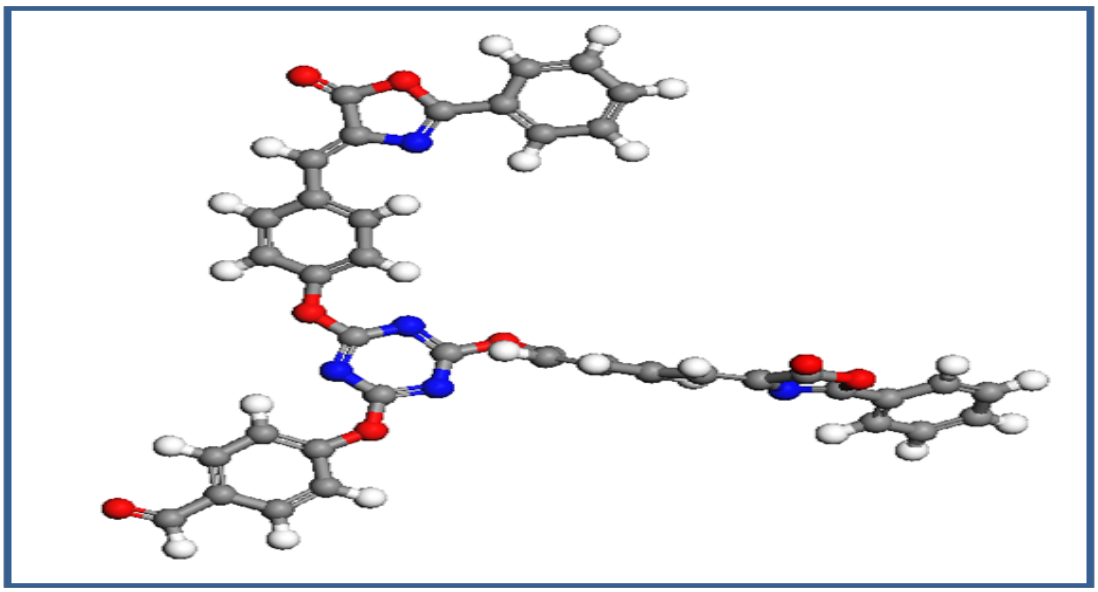

Figure. 2 The optimized molecular structure of CBOZ (5) in the XY plane

Thermal analysis

The thermal characteristics of CBOZ (5) are evaluated by TGA and DSC in the temperature range of 25-700 ºC under N_2 atmosphere at the scan rate of 10 ºC/min, as shown in Figure. 3. The thermogram of CBOZ (5) shows a little weight loss of only ~5% at around ~258 ºC, indicating a good thermal stability [36]. The TGA curve shows two stages of the compound decomposition. The first decomposition occurs in the temperature range of ~258 to ~322 ºC with a weight loss of about ~64 %, and the second stage of the decomposition with ~14% weight loss occurs at the temperature of ~700 ºC. The DSC thermogram displays two melting transition (T_m) at ~178.31 and ~271.82 ºC, indicating the liquid-crystalline (LC) property of CBOZ (5), which might be associated with the self-organization behavior due to LC-LC phase transition [37]. Also, the crystallization transition (T_c) at ~303.6 ºC might represent the self-organization of the small molecule.

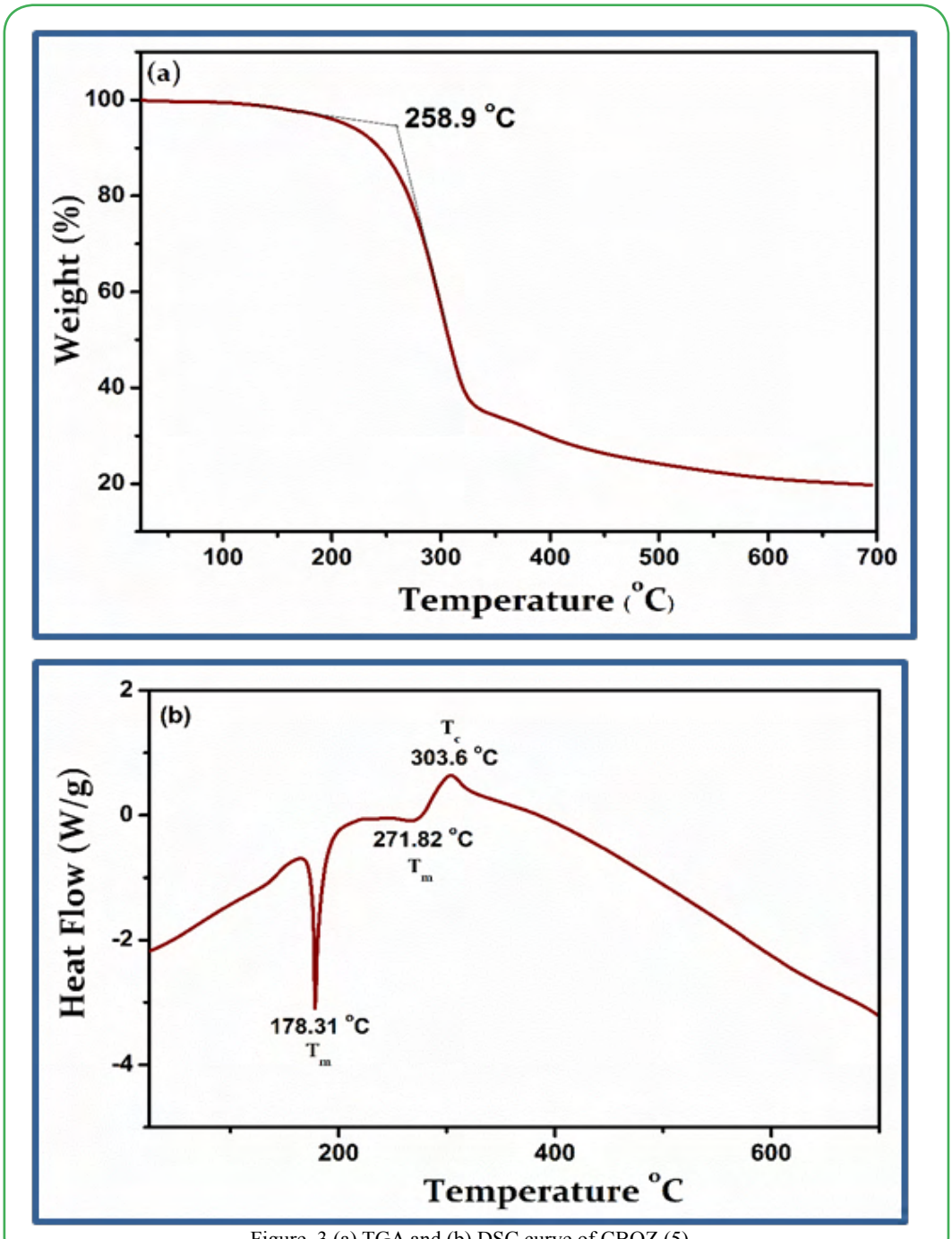

Figure. 3 (a) TGA and (b) DSC curve of CBOZ (5).

Photo-physical properties

The photo-physical properties of CBOZ (5) are investigated by UV-Vis absorption and photoluminescence (PL) emission studies. Initially, the absorption spectra of CBOZ (5) are investigated at the room temperature in 10 μM concentration of four different solvents such as chlorobenzene, chloroform, acetone and methanol. As depicted in Figure. 4(a), the absorption spectrum shows a single absorption band which corresponds to the electronic transition occurring from the π-molecular orbitals [38]. From Figure. 4(a), CBOZ (5) shows the maximum absorptivity and λmax (~370 nm) value in chlorobenzene solvent as compared to other solvents i.e. chloroform (λmax = ~367 nm), acetone (λ_{max} =~363 nm), and methanol (λ_{max} =~362 nm). Herein, the increase in the polarity of the solvent leads to the hypsochromic shift of the absorption band, indicating that CBOZ (5) is stabilized in ground state [39]. Figure. 4(b) shows the absorbance curves of CBOZ (5) in chlorobenzene of five different concentrations (such as 1, 3, 6, 8 and 10 μM). The absorbance of CBOZ (5) is performed at the room temperature which depicts an increase with the increasing

concentrations, and the maximum peak position or the wavelength for all the concentration is found as ~370 nm. These results suggest that the concentration has substantially affected the optoelectronic properties of CBOZ (5). The optical band gap (E_g) of ~3.02 eV is estimated from the equation $E_g = 1240/\lambda_{onset}$ [40].

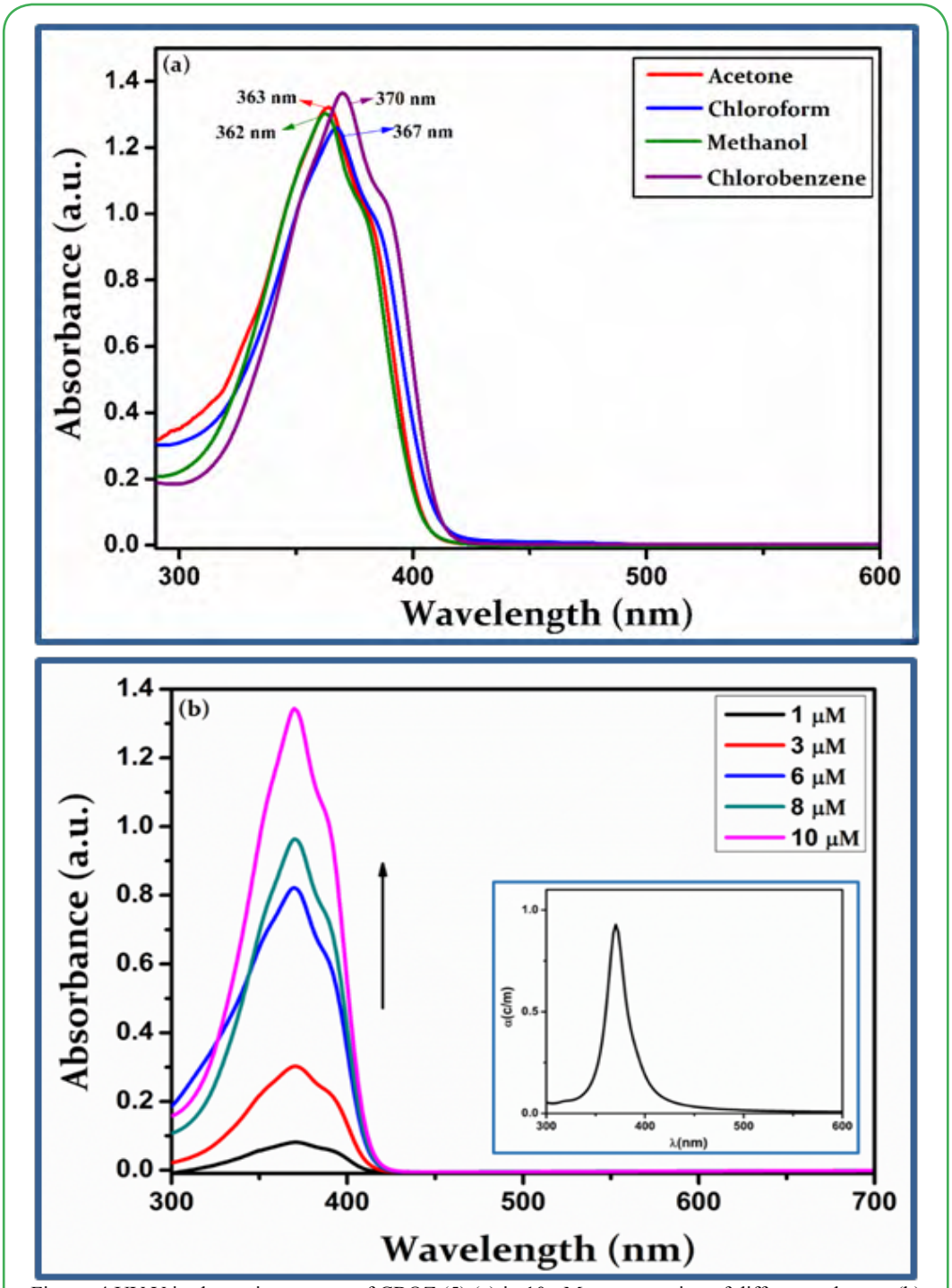

Figure. 4 UV-V is absorption spectra of CBOZ (5) (a) in 10 µM concentration of different solvents, (b) at different concentrations (1, 3, 6, 8, and 10µM) in chlorobenzene. Inset shows the simulated UV-Vis spectrum.

To get more insight into the optical properties of CBOZ (5), the PL properties are extendedly studied in 10 µM concentrations of four different solvents like chlorobenzene, chloroform, acetone and methanol at the excitation wavelength of ~380 nm. The two emission peaks at ~438 and ~553 nm are displayed, as shown in Figure. 5(a). The observed photoluminescence spectra of CBOZ (5) in the region of ~380-800 exhibits no mirror image relationship with the absorption spectra [39], which signifies the geometric rearrangement of CBOZ (5) in the excited state (S1) as compared to the initial ground state (S0). Figure. 5(a) also shows that the polarity of solvent does not affect the PL spectra of CBOZ (5), as it shows similar trends in each solvent. This might be attributed to the lack of intramolecular charge transfer (ICT) interaction within the conjugated backbone of CBOZ (5), which might lead to weak solvation effects between the solvents and the compound [41]. From Figure. 5(b), the intensity of the emission peak increases with the increase in the concentration of the compound, which evidences a strong mechanical property of CBOZ (5) [42]. Figure. 5(c) shows the emission spectra of CBOZ (5) at different excitation wavelengths ranging from 300-400 nm. The PL spectra exhibit an increase in an excitation wavelength intensity of the absorption peak, which might be related to the enlargement of π-π transitions. Moreover, with the increase of excitation wavelength, π-π excitation might be enhanced in CBOZ (5) which could increase the mechanical strength of molecules.

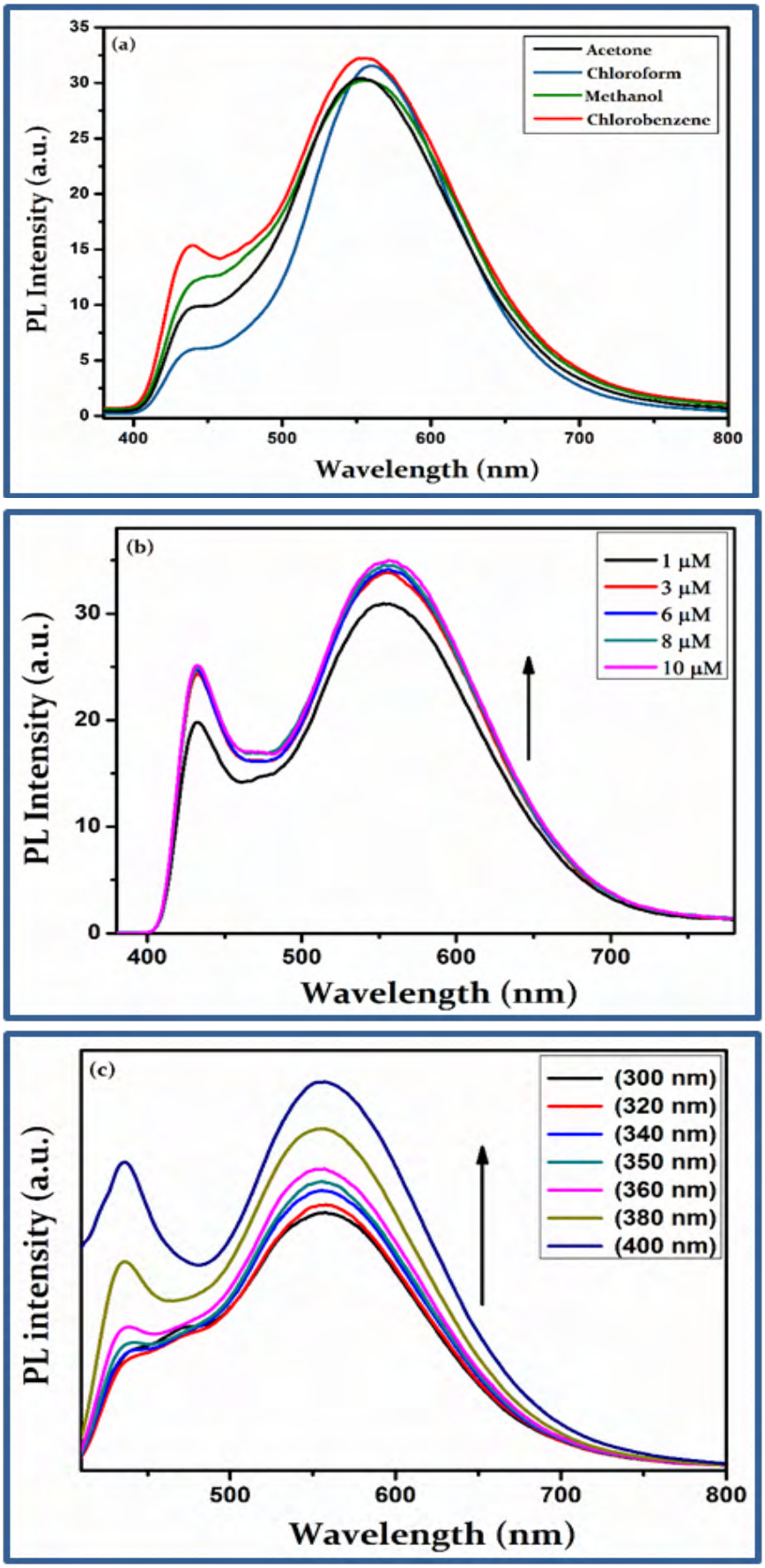

Figure. 5 PL spectra of CBOZ (5) (λ_{exc} = 380 nm) (a) in 10 μM concentration of different solvents, (b) at different concentrations (1, 3, 6, 8, and 10μM) in chlorobenzene, and (c) at different excitation wavelength (300-400 nm) with concentration of 10 μM in chlorobenzene.

Electrochemical properties

In order to explore the electrochemical behavior of CBOZ (5), the electrochemical properties are studied through CV analysis by using thin film of CBOZ (5) in 0.1 M solution of tetrabutylammonium hexaflourophosphate $[_nBu_4N]^+[PF_6]^-$ in acetonitrile at a potential scan rate of ~100 mV/s. Figure. 6(a) shows CV of CBOZ (5), and the corresponding redox potentials are summarized in Table 1. CBOZ (5) exhibits the onset oxidation potential (E_{ox}) at ~1.47 V. From the oxidation potential, the HOMO energy level as calculated by the formula [HOMO = -e (E^{ox}_{onset} + 4.40) (eV)] is found as -5.87 eV. However, the LUMO energy level is estimated as -2.85 eV by using the formula [LUMO = HUMO + E_g (eV)]. To investigate the stability of CBOZ (5), CV curve is further scanned for 25 cycles, as shown in Figure. 6(b). The multicycle CV curves displays a slightly distorted shape of CV and the peak position or the onset is marginally changed, which suggests the decent stability of CBOZ (5) in an oxidation process.

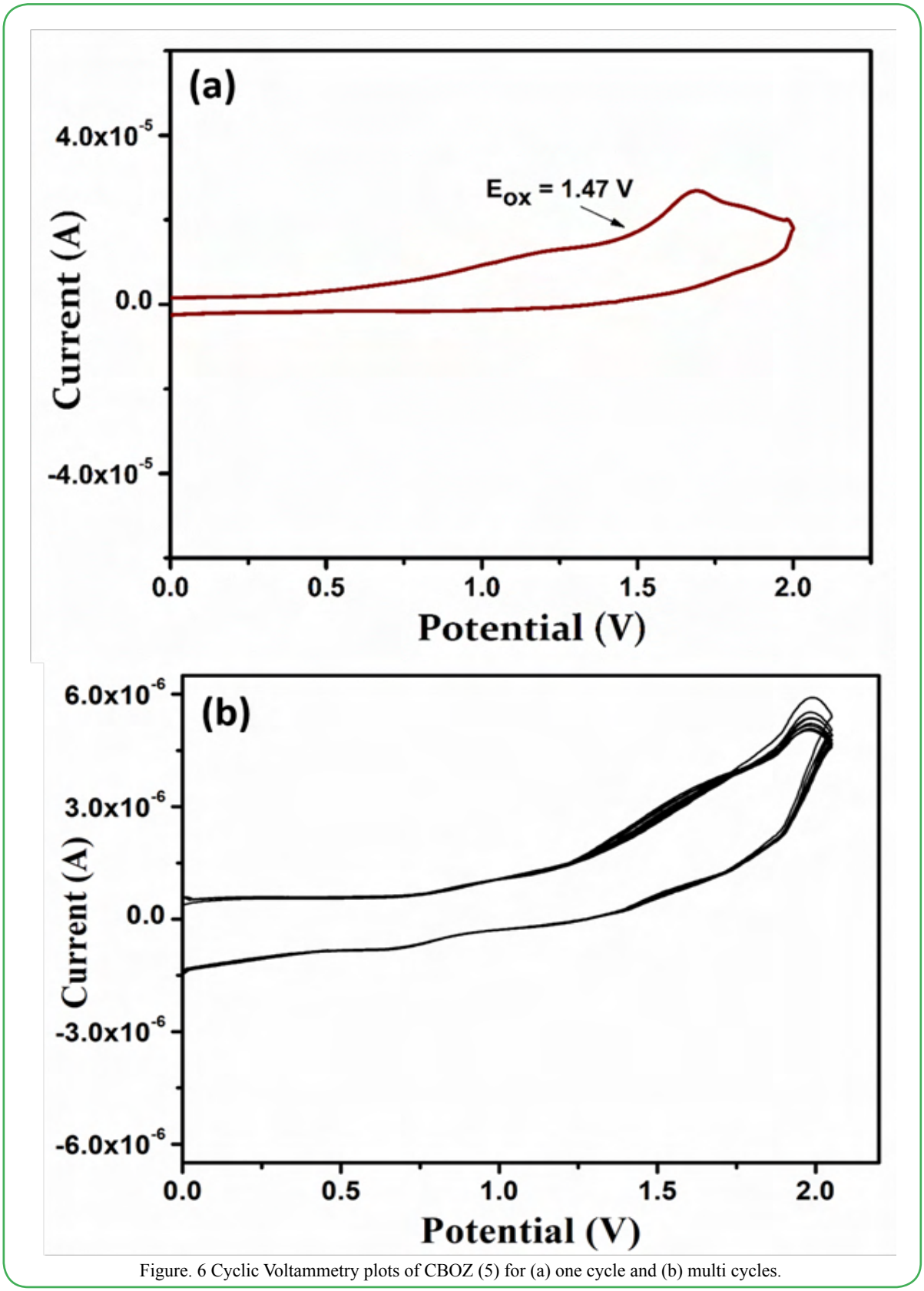

Figure. 6 Cyclic Voltammetry plots of CBOZ (5) for (a) one cycle and (b) multi cycles.

Compound 5	λ_{max}^{abs} (nm)	λ_{max}^{em} (nm)	HOMO (eV)	LUMO (eV)	E_g (eV)
Experimental	370	553	-5.87	-2.85	3.02
DFT	372	--	-5.77	-2.67	3.10

Table. 1

DFT study

In order to acquire deeper insight about the electronic spectra of CBOZ (5), density functional study (DFT) is carried out at the HSE06 functional theory and the corresponding theoretical data are compared with the experimental values, as summarized in Table 1. From UV-vis spectra (Figure. 4), the simulated UV-Vis spectrum shows a maximum absorption at wavelength of ~372 nm, which is very close to the experimental value of ~370 nm. The refractive index (n) is calculated as ~1.62. For CBOZ (5), the energy of the frontier molecular orbitals i.e. HOMO and LUMO energy levels are calculated by density functional study and are found as -5.77 and -2.67 eV, respectively, which matches well to the experimental electronic energy levels, as calculated by CV analysis. The excitation energy of HOMO→LUMO transition could be considered from the optical band gap, which is estimated as ~3.10 eV and matches well with the experimental optical band gap, as obtained from UV absorption spectrum (i.e. E_g = ~3.02 eV). The optical band gap and energy of frontier molecular orbitals describe the chemical reactivity as well as kinetic stability of the molecules [30]. The high and a low stability of the molecule could be explained by a large and small gap, respectively. Moderate E_g = ~3.02 eV value realizes that CBOZ (5) might exhibit good chemical reactivity and the kinetic properties. The spatial plots of HOMO and LUMO with energy eigen values and the optical band gaps are shown in Figure. 7. These spatial plots and low optical band gap explain the good charge transfer properties of CBOZ (5) upon excitation. In Figure. 7, the HOMO is delocalized fully over one side chain and LUMO is partially delocalized on the other side chain of triazine nucleus bearing oxazolone nucleus, which confirms the charge excitation mechanism. The charge transfer is noticed from one substituted chain to other upon HOMO→LUMO excitation.

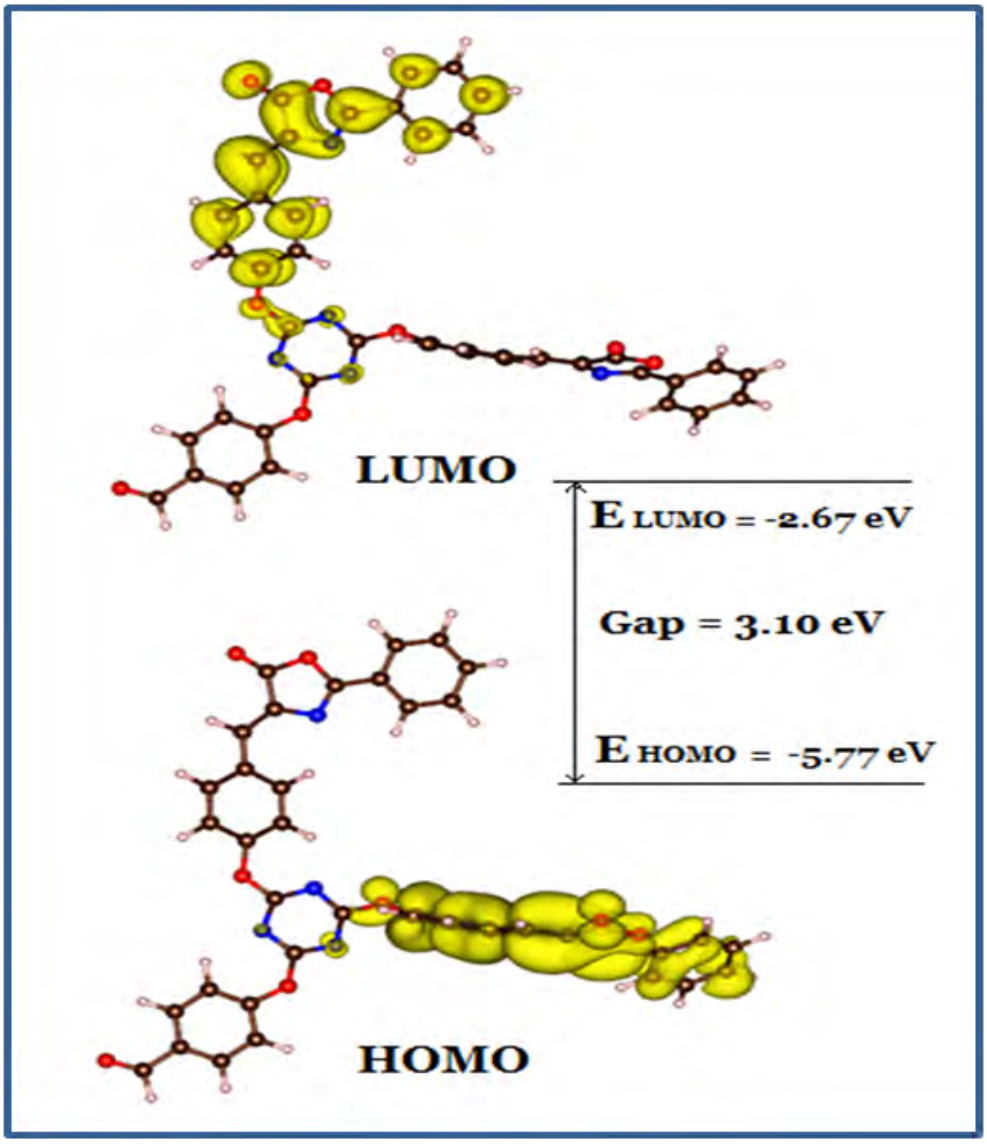

Figure. 7 HOMO and LUMO plots for CBOZ (5)

Conclusions

In summary, a new and novel oxazolone molecule, CBOZ (5) with central triazine nucleus substituted with two oxazolone ring is successfully synthesized by two step reactions and characterized extensively by FTIR, ^{1}H NMR, ^{13}C NMR and MS spectroscopic analysis. CBOZ (5) exhibits relatively a good thermal stability, as observed by the decomposition temperature of ~258 ºC. The synthesized CBOZ (5) displays a reasonable good optical band gap with the HOMO of ~ -5.87 eV and LUMO of ~ -2.85 eV. The photoluminescence properties reveal that the significant mechanical strength of CBOZ (5) increases with the increase of the concentration and excitation wavelengths. Importantly, the optical and electrochemical studies of CBOZ (5) are comprehensibly consistent with the DFT calculated optical band gaps and HOMO and LUMO energy levels.

Conflict of interests

The authors declare that there is no conflict of interests regarding the publication of this paper.

Acknowledgements

Sadia Ameen acknowledges NRF Project #2016R1D1A1B03934446. This work is also supported by NRF Project #2017R1A2B2003381. We acknowledge the Korea Basic Science Institute, Jeonju branch, for utilizing the research supported facilities.

References

1. Tsai MH, Hong YH, Chang CH, Su HC, Wu CC et al. (2007) 3-(9-Carbazolyl)carbazoles and 3,6-di(9-carbazolyl) carbazoles as effective host materials for efficient blue organic electrophosphorescence, Adv Mater 19: 862-866.
2. Hu ZJ, Yang JX, Tian YP, Zhou HP, Tao XT et al. (2007) Synthesis and optical properties of two 2,2′: 6′,2″-terpyridyl-based two-photon initiators, J Mol Struct 839: 50-57.
3. Parveen M, Malla AM, Alam M, Ahmad F, P. Silva PSP et al. (2014) Two new phenolic compounds from Ficus rumphii and their antiproliferative activity, Nat Prod Res 28: 646-652.
4. Gondek E, Kityk IV, Danel A, Wisla A, Sanetra J et al. (2006) Blue electroluminescence in 1H-pyrazoloquinoline derivatives, Synth Met 156: 1348-1354.
5. Ahmad F, Alam MJ, Alam M, Azaz S, Parveen M et al. (2018) Synthesis,spectroscopic, computational (DFT/B3LYP), AChE inhibition and antioxidant studies of imidazole derivative, J Mol Str 1151: 327-342.
6. Parveen M, Ahmad F, Malla AM, Azaz S (2015) SiO2-H3BO3 promoted solvent-free, green and sustainable synthesis of bioactive 1-substituted-1H-tetrazole analogues, New J Chem 39: 2028-2041.
7. Gottwald K, Seebach D (1999) Ring opening with kinetic resolution of azlactones by Ti-TADDOLates, Tetrahedron 55: 723-738.
8. Khadse SC, Chatpalliwar VA (2017) Synthesis of benzamides by microwave assisted ring opening of less reactive dimethylaminobenzylidene oxazolone, Arab J Chem 10: S859-S863.
9. Cavalier F, Verducci J (1995) New synthesis of the cyclic tetrapeptide tentoxin employing an azlactone as key intermediate, Tetrahedron Lett 36: 4425-4428.
10. Park BS, Oh CM, Chun KH, Lee JO (1998) Photoinduced one pot transformation of 2-phenyl-4-ethylidene-5(4H)-oxazolone and allylic alcohols to γ,δ-unsaturated N-benzoyl amides, Tetrahedron Lett 39: 9711-9714.
11. Bates RB, Janda KD (1984) A convenient synthesis of α-acylamino alcohols from azlactones, Synthesis 1984: 310.
12. Bossio R, Marcaccini S, Pepino R, Paoli P (1994) Studies on isocyanides and related compounds. An unusual synthesis of imidazolyloxazolones, J Heterocycl Chem 31: 729-732.
13. Tandon M, Coffen DL, Gallant P, Keith D, Ashwell MA et al. (2004) Potent and selective inhibitors of bacterial methionyl tRNA synthetase derived from an oxazolone-dipeptide scaffold, Bioorg. Med Chem Lett 14: 1909-1911.
14. Sierra FMP, Pierre A, Burbridge M, Guilbaud N (2002) Novel bicyclic oxazolone derivatives as anti-Angiogenic agents, Bioorg. Med Chem Lett 12: 1463-1466.
15. Parveen M, Ali A, Ahmed S, Malla AM, Alam M et al. (2013) Synthesis, bioassay, crystal structure and ab initio studies of Erlenmeyer azlactones, Spectrochim. Acta, Part A 104: 538-545.
16. Goksen US, Kelekci NG, Goktas O, Koysal Y, Kilic E et al. (2007) 1-Acylthiosemicarbazides, 1,2,4-triazole-5(4H)-thiones, 1,3,4-thiadiazoles and hydrazones containing 5-methyl-2-benzoxazolinones: Synthesis, analgesic, anti-inflammatory and antimicrobial activities Bioorg. Med Chem 15: 5738-5751.
17. Madkour HMF (2002) Simple one-step syntheses of heterocyclic systems from (4Z)-2-phenyl-4-(thien-2-ylmethylene)-1,3(4H)-oxazol-5-one, Chem Pap 56: 313-319.
18. Tsukumo Y, Harada D, Manabe H (2010) Pharmacological characterization of itch-associated response induced by repeated application of oxazolone in mice, J Pharmacol Sci 113: 255-262.
19. Hamidian H, Azizi S (2015) Synthesis of novel compounds containing morpholine and 5(4H)-oxazolone rings as potent tyrosinase inhibitors, Bioorg Med Chem 23: 7089-7094.
20. Mohamed LW, El-Badry OM, El-Ansary AK, Ismael A (2017) Design & synthesis of novel oxazolone & triazinone derivatives and their biological evaluation as COX-2 inhibitors, Bioorg Chem 72: 308-314.
21. Ozturk G, Alp S, Timur S (2008) Photophysical characterization of fluorescent oxazol-5-one derivatives in PVC and their application as biosensors in the detection of ACh and AChE inhibitor: Donepezil, Dye Pigment 76: 792-798.
22. Ozturk G, Alp S, Ertekin K (2007) Fluorescence emission studies of 4-(2-furylmethylene)-2-phenyl-5-oxazolone embedded in polymer thin film and detection of Fe3+ ion, Dye Pigment 72: 150-156.
23. Murthy YLN, Christopher V, Prasad UV, Bisht PB, Ramanaih DV et al. (2010) Synthesis and study of nonlinear optical properties of 4-substituted benzylidene-2-phenyl oxazol-5-ones by Z-scan technique Synth. Metals 160: 535-539.
24. Bourotte M, Schmitt M, Wund AF, Pigault C, Haiech J et al. (2004) Fluorophores related to the green fluorescent protein, Tetrahedron Lett 45: 6343-6348.
25. Jung B, Kim H, Park BS (1996) Photodecarbonylation of 2-phenyl-4-alkylidene-5(4H)-oxazolones, Tetrahedron Lett. 37: 4019-4022.
26. Ertekin K, Alp S, Karapire C, Yenigul B, Henden E et al. (2000) Fluorescence emission studies of an azlactone derivative embedded in polymer films: An optical sensor for pH measurements, J. Photochem. Photobiol. A: Chem 137: 155-161.
27. Gonzalez AF, Badia R, Garcia MED (2005) Insights into the reaction of β-lactam antibiotics with copper (II) ions in aqueous and micellar media: Kinetic and spectrometric studies, Anal Biochem 341: 113-121.
28. Murthy YLN, Suhasini KP, Veeraiah V, Umesh G, Manjunatha KB et al. (2013) Synthesis, characterization and evaluation of the photophysical and nonlinear optical behaviour of novel 4-substituted arylidene-2-[5-(2,6-dichlorophenyl)-3-methyl-1,2-oxazol-4-yl]-1,3-oxazol-5-ones, Dyes Pigments 99: 713-719.

29. Ozturk G, Alp S, Ergun Y (2007) Synthesis and spectroscopic properties of new 5-oxazolone derivatives containing an N-phenyl-aza-15-crown-5 moiety, Tetrahedron Lett 48: 7347-7350.
30. Kresse G, Hafner J (1993) Ab initio molecular dynamics for liquid metals, Phys Rev B 47: 558-561.
31. Kresse G, Furthmüller J (1996) Efficient iterative schemes for ab initio total-energy calculations using a plane-wave basis set, Phys Rev B 54: 11169-11186.
32. Kresse G, Joubert D (1999) From ultrasoft pseudopotentials to the projector augmented-wave method, Phys Rev B 59: 1758-1775.
33. Grimme S (2006) Semiempirical GGA-type density functional constructed with a long-range dispersion correction, J Comput Chem 27: 1787-1799.
34. Mikroyannidis JA, Sharma SS, Vijay YK, Sharma GD (2010) Novel low band gap small molecule and phenylenevinylene copolymer with cyanovinylene 4-nitrophenyl segments: synthesis and application for efficient bulk heterojunction solar cells, ACS Appl Mater Interfaces 2: 270-278.
35. Parveen M, Ahmad F, Malla AM, Azaz S, Silva MR et al. (2015) [Et3NH][HSO4]-mediated functionalization of hippuric acid: an unprecedented approach to 4-arylidene-2-phenyl-5(4H)-oxazolones, RSC Adv 5: 52330-52346.
36. Zhang J, Yin P, Xu L, Shen P, Ye M et al. (2018) Photovoltaic molecules based on vinylene-bridged oligothiophene applied for bulk-heterojunction organic solar cells, J. Energy Chem 27: 426-431.
37. Nazim M, Ameen S, Akhtar MS, Shin HS (2018) Asymmetric, efficient π-conjugated organic semiconducting chromophore for bulk-heterojunction organic photovoltaics, Dye Pigment 149: 141-148.
38. Ortega HB, Guerra LJ, Lima SR, Huizar LHM, R.A.V. Garcia RAV et al. (2018) One pot synthesis, X-ray crystal structure of 2-(2′-hydroxyphenyl)oxazolo[4,5-b]pyridine derivatives and studies of their optical properties, J Mol Str 1157: 119-126.
39. Somasundaram S, Kamaraj E, Hwang SJ, Park S (2018) Structural, photophysical, and theoretical studies of imidazole-based excited-state intramolecular proton transfer molecules, Spectrochim. Acta Part A 191: 325-335.
40. Feng H, Qiu N, Wang X, Wang Y, Kan B (2017) An A-D-A type small-molecule electron acceptor with end-extended conjugation for high performance organic solar cells, Chem Mater 29: 7908-7917.
41. Chen G, Li X, Chen Z, Tang C, Yang W et al. (2018) Synthesis, optical and electrochemical properties of polycyclic aromatic compounds based on bis(benzothiophene)-fused fluorene, C. R. Chim..
42. Wang C, Li Z (2017) Molecular conformation and packing: their critical roles in the emission performance of mechanochromic fluorescence materials, Mater Chem Front 1: 2174-2194.